Effects of energetic particle phase space modifications by instabilities on integrated modeling

IOP Publishing | International Atomic Energy Agency Nuclear Fusion

Nucl. Fusion **56** (2016) 112005 (11pp) doi:10.1088/0029-5515/56/11/112005

Effects of energetic particle phase space modifications by instabilities on integrated modeling

M. Podestà, M. Gorelenkova, E.D. Fredrickson, N.N. Gorelenkov and R.B. White

Princeton Plasma Physics Laboratory, Princeton, NJ 08543, USA

E-mail: mpodesta@pppl.gov

Received 16 January 2016, revised 6 April 2016
Accepted for publication 11 April 2016
Published 22 July 2016

Abstract

Tokamak plasmas can feature a large population of energetic particles (EP) from neutral beam injection or fusion reactions. In turn, energetic particles can drive instabilities, which affect the driving EP population leading to a distortion of the original EP distribution function and of quantities that depend on it. The latter include, for example, neutral beam (NB) current drive and plasma heating through EP thermalization. Those effects must be taken into account to enable reliable and quantitative simulations of discharges for present devices as well as predictions for future burning plasmas. Reduced models for EP transport are emerging as an effective tool for long time-scale integrated simulations of tokamak plasmas, possibly including the effects of instabilities on EP dynamics. Available models differ in how EP distribution properties are modified by instabilities, e.g. in terms of gradients in real or phase space. It is therefore crucial to assess to what extent different assumptions in the transport models affect predicted quantities such as EP profile, energy distribution, NB driven current and energy/momentum transfer to the thermal populations. A newly developed *kick model*, which includes modifications of the EP distribution by instabilities in both real and velocity space, is used in this work to investigate these issues. Coupled to TRANSP simulations, the kick model is used to analyze NB-heated NSTX and DIII-D discharges featuring unstable Alfvén eigenmodes (AEs). Results show that instabilities can strongly affect the EP distribution function, and modifications propagate to macroscopic quantities such as NB-driven current profile and NB power transferred to the thermal plasma species. Those important aspects are only qualitatively captured by simpler fast ion transport models that are based on radial diffusion of energetic ions only.

Keywords: NB current drive, fast ion transport modeling, integrated tokamak simulations, TRANSP code

(Some figures may appear in colour only in the online journal)

1. Introduction

Enhanced fast ion transport caused by instabilities can be detrimental for the operation of fusion devices such as ITER and a Fusion Nuclear Science Facility [1]. Increased fast ion redistribution and losses reduce the fusion efficiency, affect the controllability and predictability of quantities such as neutral beam (NB) driven current and may cause harm to in-vessel structures. It is therefore important to develop and validate modeling tools that enable accurate predictions of fast ion transport in future devices, including the effects of plasma instabilities.

In this work, the TRANSP [2, 3] tokamak transport code is used for integrated simulations of discharges from the NSTX spherical torus [4] and the DIII-D tokamak [5]. The main goal is to investigate whether—and for which quantities—a detailed

modeling of the fast ion distribution function is required to obtain quantitatively meaningful results even when MHD instabilities are destabilized. It is anticipated that simple, ad hoc diffusive models can already capture global features that are good indicators of a discharge performance, such as neutron rate, stored energy and overall NB current drive efficiency. However, a more rigorous treatment of the fast ion distribution evolution appears to be required to account for radial and temporal variations of integrals of the fast ion distribution. Examples include modeling of the NB driven current profile and contribution to the local power balance from the thermalizing fast ions.

The remainder of the paper is organized as follows. The modeling tools used in this work are introduced in section 2, followed by a description of the target NSTX and DIII-D scenarios in section 3. The main results of this study are then described in section 4. Section 5 concludes the paper with a discussion of the main findings and their implications for future research.

2. Modeling tools and analysis procedure

The main numerical tool used for the whole-discharge integrated simulations considered herein is the tokamak transport code TRANSP [2, 3]. Input profiles from the experiments include electron/ion density/temperature, q-profile, plasma toroidal rotation and magnetic equilibrium from the EFIT code [6, 7]. Other quantities are constrained based on experimental measurements, such as total plasma current, surface voltage and NB injection parameters (active sources, geometry, injected power and current).

The NUBEAM module implemented in TRANSP models the fast ion evolution based on classical fast ion physics [8, 9]. Several options are available in NUBEAM to account for fast ion transport mechanisms other than classical. Commonly used transport models are based on ad hoc diffusion and convection coefficients, which result in radial fast ion transport proportional to the local fast ion density gradient and density. In addition to the ad hoc models, a physics-based reduced model (*kick model* [10]) has been recently implemented in TRANSP [11]. Contrary to the ad hoc models of NUBEAM, the *kick model* accounts for the interaction of fast ions with instabilities in phase space, here represented through energy, canonical toroidal momentum and magnetic moment (E, P_ζ and μ respectively) following [12]. The model is based on a transport probability $p(\Delta E, \Delta P_\zeta | E, P_\zeta, \mu)$ associated to regions of phase space identified by E, P_ζ, μ. The probability describes changes (or *kicks*) in particle's energy and toroidal canonical momentum, ΔE and ΔP_ζ, resulting from fast ion interaction with instabilities [10]. n this work, a separate probability is computed for each mode included in the analysis. Up to 10 different modes can be modeled in a TRANSP run (note that this number has been increased with respect to previous works, e.g. [10, 11]). The transport matrix is computed through particle-following codes such as ORBIT [13]. Perturbations used in ORBIT are modeled by MHD codes such as NOVA [14–16] that reproduce experimentally observed instabilities in terms of frequency and mode number spectrum. The mode structure is assumed to be independent of the mode amplitude and of the EP drive, i.e. EP effects altering the ideal MHD mode structure are not accounted for. In the spirit of the reduced modeling approach adopted in this work, this appears as a reasonable approximation. For instance, previous comparisons of measured mode structures with predictions from NOVA showed reasonable agreement, see [17–19]. After an initial verification against the ORBIT code [10], the new model is now being tested against NSTX and DIII-D data [20]. Initial results compare well with experimental results and with predictions from a *critical gradient* model [21].

3. Experimental scenarios

The discharges analyzed in this study have been selected to encompass a variety of NB-heated plasma scenarios, including L- and H-mode plasmas, ramp-up scenarios and high-$q_{\min}$, nearly steady-state discharges (see figure 1 and table 1). All discharges feature robust Alfvénic activity. Dominant modes are identified as toroidal and reverse-shear Alfvén eigenmodes (TAEs and RSAEs) based on their frequency, frequency evolution and mode structure. The latter is computed through the ideal MHD code NOVA, matching the measured frequency and (toroidal) mode numbers. (Details on the NOVA analysis can be found in [18]). Other instabilities such as kink-like modes and tearing modes, are present in some cases. DIII-D discharges also feature elliptical AEs at higher frequency than TAEs and RSAEs (see, for example, the spectrum for DIII-D discharge #153072 in figure 1). Kink-like, low-frequency AEs and NTMs are included in the analysis. Since no direct experimental information is available, their mode structure is modeled through simplified analytical expressions similar to that used in [22], with toroidal spectrum and frequency as observed in the experiments. EAEs are not included since, according to ORBIT simulations, they would cause only marginally incremental transport of energetic particles with respect to TAEs/RSAEs and lower frequency modes.

For each discharge, three TRANSP runs are performed to compile a database with relevant quantities such as neutron rate, stored energy, NB driven current and fast ion density. The three runs refer to *classical* analysis, i.e. without any additional fast ion transport included; analysis with a time-dependent, spatially uniform fast ion diffusivity (called ad hoc *model* in the following and in the figures); analysis with the phase space resolved *kick model* to simulate fast ion transport. The database is obtained by binning the quantities of interest (e.g. neutron rate, NB driven current, NB ion density) every 10 ms. Error bars shown in the figures refer to the standard deviation of the different quantities within the 10 ms time window. Error bars do not include possible systematic errors from the experimental measurements. The database results are restricted to a time range around the reference time at which the probabilities $p(\Delta E, \Delta P_\zeta)$ are computed. The selection is based on the stationarity of the plasma profiles, and in particular of the safety factor. Only time points for which central and minimum q are within ± 1 of their values at the reference

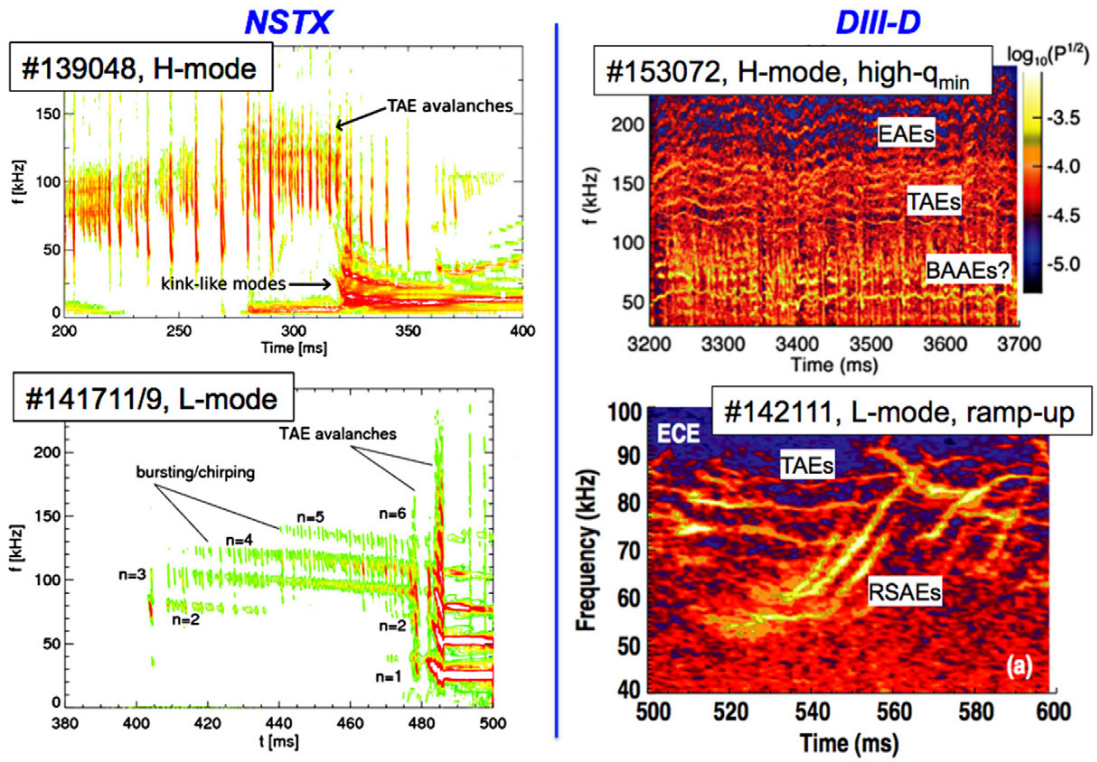

Figure 1. Frequency spectra as a function of time for the discharges investigated herein. Data are from pickup Mirnov coils located at the vessel wall for NSTX and from CO2 reflectometer and ECE radiometer data for DIII-D.

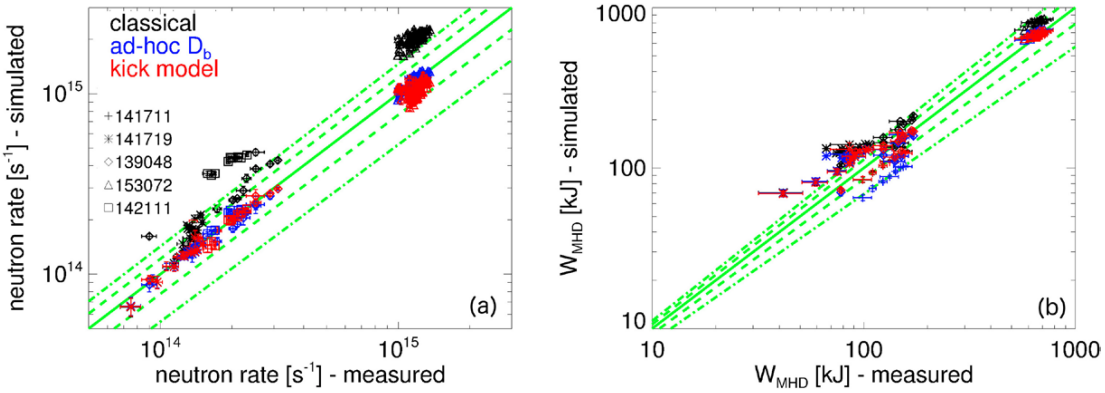

Figure 2. Comparison of (*a*) neutron rate and (*b*) stored energy computed by TRANSP against experimental values. Simulations are run with different assumptions for fast ion transport (classical physics; ad hoc diffusion; kick model). Here and in the following figures the solid, dashed and dot–dashed lines refer to $1:1, 1:1\pm25\%$ and $1:1\pm50\%$ correspondence, respectively.

Table 1. Summary of NSTX and DIII-D discharges analyzed in this work.

Device	Shot no.	Time (ms)	B_0 (T), I_p (MA)	Confinement	Instabilities	References
NSTX	139048	200–325	0.45, 0.9	H-mode	RSAEs, TAEs, kink	[10, 11, 18, 23]
NSTX	141711	415–485	0.5, 0.9	L-mode	TAEs, kink	[19, 24, 25]
NSTX	141719	355–525	0.5, 0.9	L-mode	TAEs, kink	[19, 24, 25]
DIII-D	142111	425–585	2.0, ramp-up	L-mode	RSAEs, TAEs	[26–29]
DIII-D	153072	2600–3485	1.8, 2	H-mode	TAEs, EAEs, low-f AEs, NTM	[30, 31]

Note: More details on each discharge are given in the references (last column).

time for NOVA and ORBIT analysis are retained in the following analysis.

For the ad hoc model, the diffusivity D_b is adjusted as a function of time to match the evolution of measured neutron rate and stored energy (W_{MHD}, reconstructed through the EFIT code for equilibrium reconstruction [6, 7]), see figure 2. So-called *partial kinetic* EFIT runs [32, 33], based on measured thermal ion/electron pressure and an estimated fast ion pressure, provide the constraint for the reconstructed total stored energy. Reconstructions do not include the effects of pressure anisotropy. The corresponding W_{MHD} term in TRANSP is computed based on the input density and temperature profiles for thermal electrons and ions, plus the contribution from the EP population resulting from the NUBEAM module. Note that, even if the effects of instabilities on energetic particle transport are introduced through the ad hoc D_b or kick models, the electromagnetic energy associated with instabilities is not accounted for in W_{MHD}. In practice, there are cases for which good agreement can be achieved for only one of the above mentioned quantities. In those cases, priority is given to match the neutron rate, at the expenses of some mismatch between simulated and reconstructed W_{MHD}. A similar procedure is here adopted to adjust the amplitude scaling factor for each mode included in the kick model. Starting from the experimental mode amplitude (when available), corrections are applied iterating the TRANSP runs to optimize the match with neutron rate and W_{MHD}. Results of this procedure are also shown in figure 2, which compares the measured neutron rate and W_{MHD} (as reconstructed by EFIT) with the results for the three TRANSP runs for all discharges in the database.

Not surprisingly, *classical* runs over-estimate both neutron rate and stored energy with respect to the experiments. That indicates that classical runs over-predict the fast ion content in the plasma. In the experiments, fast ion transport is enhanced by instabilities, resulting in degraded fast ion confinement and therefore lower neutron rate and stored energy. Note that, since thermal plasma profiles are given as input, changes in the total W_{MHD} are caused by fast ion transport only. Overall, both the ad hoc and *kick* models are capable to recover the drop in the measured quantities within the experimental uncertainties (typically of the order of $\pm 5\%$, neglecting systematic errors in the measurements), as illustrated in figure 2. The next sections assess the resulting changes in other important quantities that are usually derived through integrated simulations.

4. Results from combined NSTX and DIII-D database

A first result from the combined NSTX/DIII-D analysis is presented in figure 3. The NB current drive efficiency with respect to classical simulations is shown as a function of the inferred deficit in neutron rate, defined as the relative departure of computed neutron rate from predictions assuming classical fast ion behavior. Since the deficit is roughly proportional to the amount of Alfvénic activity (see, for instance, figures 8–10 in [30]), the abscissa in figure 3 can be taken as an indicator of the severity of the instabilities. NB current drive efficiency is here defined as the ratio of NB driven current carried by fast ions (see [34, 35] for its complete definition in TRANSP) to the total current, normalized to the injected NB power.

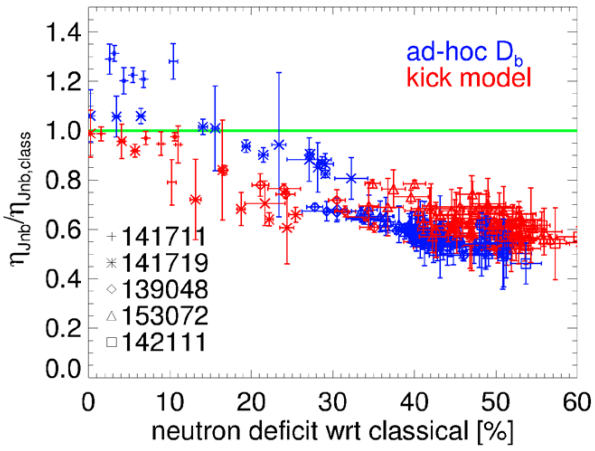

Figure 3. NB current drive efficiency, normalized to the *classical* case, as a function of the measured deficit in neutron rate with respect to classical simulations. Results from the two fast ion transport models (ad hoc diffusivity and kick model) are shown. Here and in the following figures, data points from each discharge are shown with different symbols as per the legend in the figure.

For the cases considered herein, up to 60% neutron rate deficit is observed. The corresponding reduction of NB current drive efficiency is 20–60%. This large reduction indicates that these effects must certainly be taken into account for accurate, quantitative modeling and interpretation of the experimental data. From figure 3, differences are observed in the values predicted by using either the ad hoc diffusion or the kick model to account for enhanced fast ion transport by instabilities. This suggests that a correct treatment of the fast ion evolution is required, possibly including phase space effects when resonant instabilities are observed.

4.1. Modifications of the fast ion distribution function

A critical indicator of the effects of instabilities on the fast ion population is provided by the fast ion distribution function, here computed by the NUBEAM module of TRANSP. Figure 4 shows an example from a NSTX discharge with unstable TAEs that develop into so-called avalanches, i.e. large amplitude bursts of the modes followed by drops in the measured neutron rate and enhanced losses. Effects of the instabilities are clearly not taken into account in the classical TRANSP run, which is taken as reference for the analysis with the two other transport models.

Consistent with the decrease in neutron rate and stored energy, additional fast ion transport causes a reduction in the core fast ion content. Significant differences are observed when the simple diffusive model or the kick model are used, see figure 4 for an example from NSTX discharge #139048. When uniform radial diffusion is applied, the entire distribution is reduced by a similar amount, regardless of the energy or pitch of the fast particles. For the kick model, however,

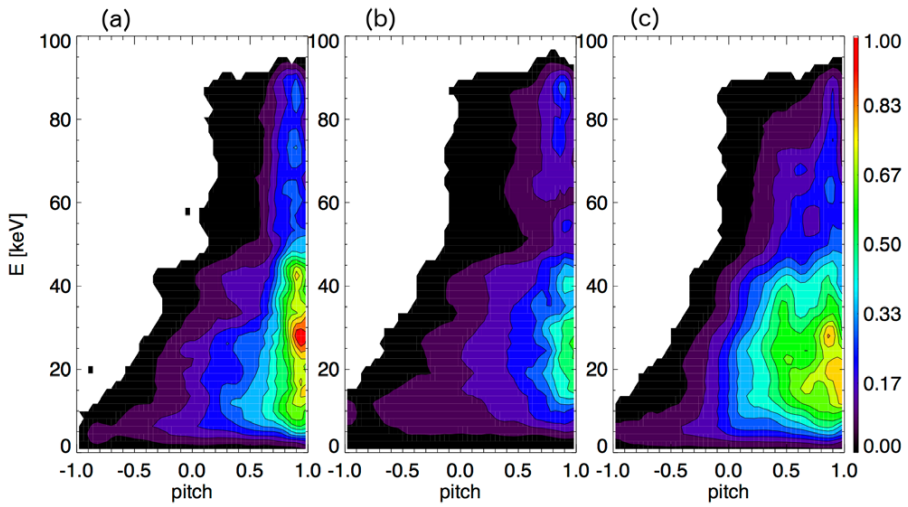

Figure 4. Example of fast ion distribution functions around $r/a \sim 0.5$ as a function of energy and pitch (ratio of parallel to total velocity) under different assumptions for fast ion transport mechanisms: (*a*) classical, (*b*) ad hoc diffusion, (*c*) kick model. Note the broadening of the distribution in panel (*c*), resulting from particles with large pitch being pushed to smaller pitch values by instabilities.

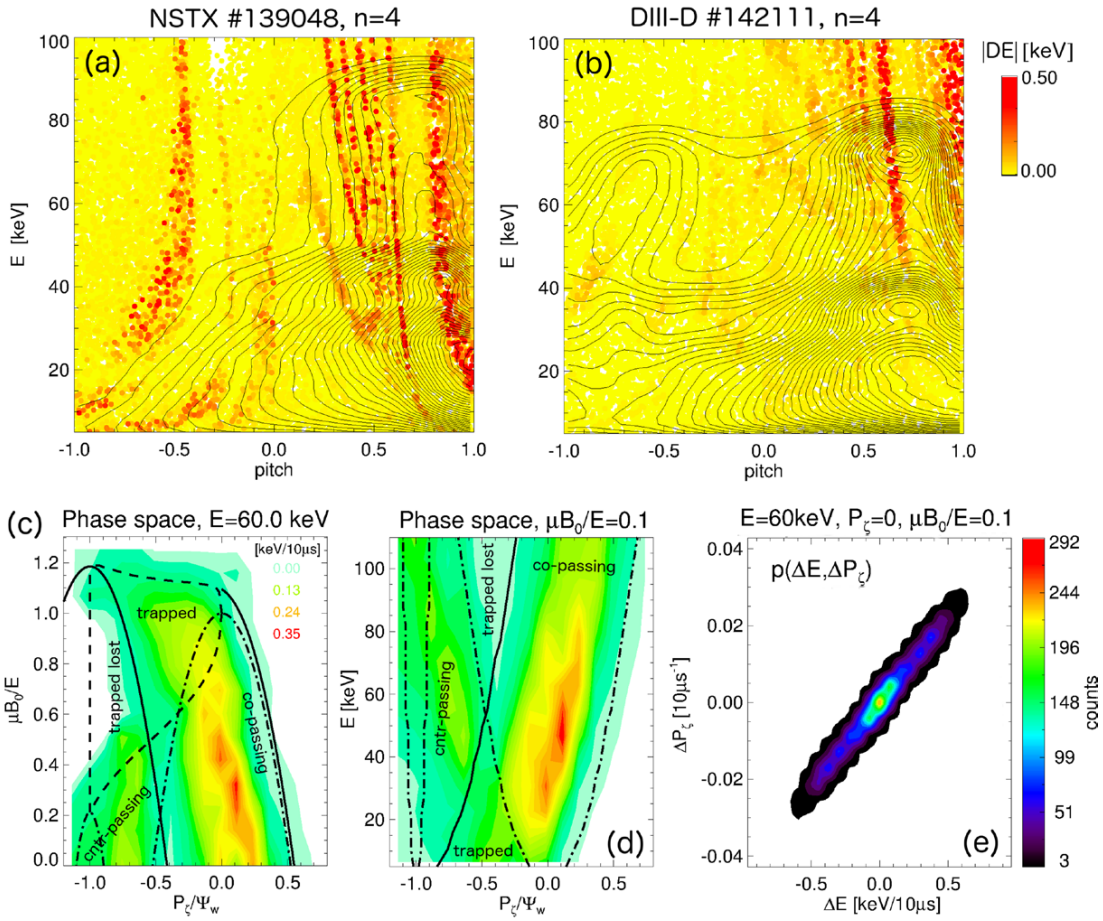

Figure 5. ORBIT results showing resonant particles initialized at midplane, whose energy is modified over a 0.5 ms simulation, at $r/a \sim 0.4$ (location of peak mode amplitude) for (*a*) NSTX discharge #139048 and (*b*) DIII-D discharge #142111. (*E* and pitch variables refer to the initial particles' energy and pitch.) For each discharge, a single mode with multiple poloidal harmonics is used in ORBIT. Contour lines show the fast ion distribution as computed for *classical* TRANSP runs. ((*c*) and (*d*)) Phase-space representations of panel (*a*) showing the root-mean-square energy kicks as a function of constants of motion. Orbits are classified as per [12]. (*e*) Kick probability $p(\Delta E, \Delta P_\zeta)$ from panels ((*c*) and (*d*)) for co-passing particles with $E = 60$ keV, $P_\zeta \approx 0$ and $\mu B_0/E = 0.1$.

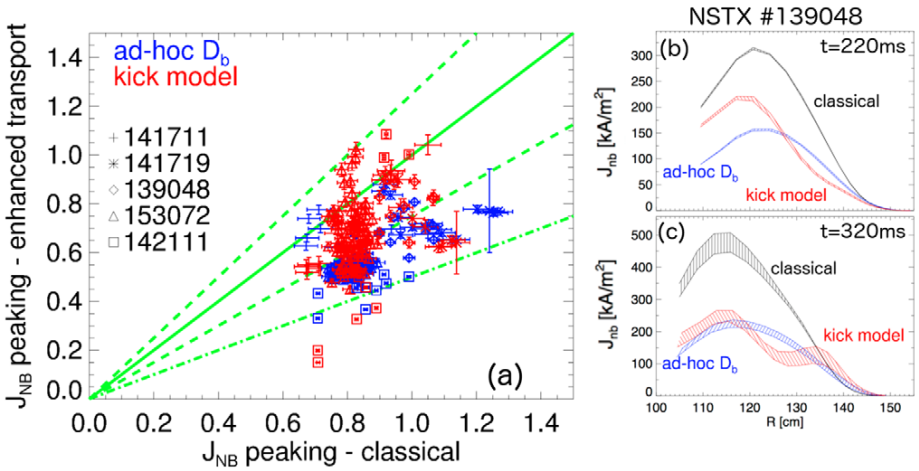

Figure 6. (*a*) Comparison of NB-driven current peaking factor from runs using ad hoc diffusion or kick model with respect to classical simulations. Overall, enhanced fast ion transport results in a decrease in current peaking, i.e. broader NB-driven current profiles. ((*b*) and (*c*)) Although average quantities such as the peaking factor are similar, the radial profiles of J_{NB} and their temporal variations can differ substantially between the two models.

some regions of the distribution suffer a larger depletion than others. More specifically, for the dominant TAE/RSAEs present in the selected discharges, higher energy co-passing particles are transported more efficiently. This is consistent with the fact that co-passing particles are the ones resonating more efficiently with the instabilities, and therefore are more prone to be affected by the modes. Examples of the location of resonances in the (E, pitch) variables are shown in figure 5. Because of the high ratio of fast ion to Alfvén velocity, v_f/v_A, resonances on NSTX can extend to low energies, $E \sim 20$ keV or below. For typical NB injection parameters, resonance locations and the EP distribution mostly overlap at pitch $\geqslant 0.5$, corresponding to co-passing particles. Because of the higher magnetic field DIII-D scenarios are characterized by a lower v_f/v_A ratio and resonances are effective at higher energies than on NSTX, see figure 5(*b*). (Typical NB injection energies are comparable for the two devices).

Contrary to the rather uniform modification of the distribution function for the ad hoc model, the kick model can result in more complex distortions of the original (classical) distribution. Several mechanisms compete: (i) changes in particle's energy and P_ζ (and, therefore, of radius since $P_\zeta = P_\zeta(\Psi)$, with Ψ: poloidal flux) caused by instabilities, which will tend to flatten local gradients in energy and P_ζ; (ii) classical pitch angle scattering and slowing down. For example, comparing figuers 4(*c*) and 5(*a*) for NSTX discharge #139048, the kick model mostly affects resonant particles along the (almost vertical) resonances seen in figure 5(*a*). Outside the resonant regions, the effect of kicks is much weaker, at most comparable to that of collisions (slow-down and pitch-angle scattering). The net effect is, for this example, a broadening of the distribution at energies $E \geqslant 10$–20 keV which then propagates to lower energies as particles slow down. Note that, for fast ion orbits, neither Ψ nor the pitch parameter $v_\parallel/v$ are constants of motion. Both parameters can experience significant variations during a particle's orbit, especially when instabilities are present. Deviations from the initial values are

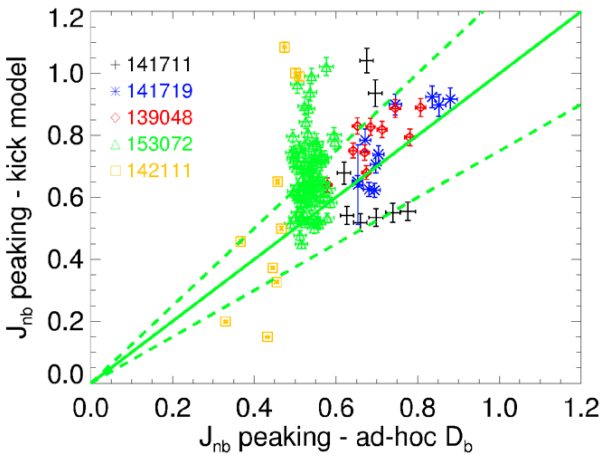

Figure 7. Comparison between J_{NB} peaking factor from the ad hoc D_b and kick models. Overall, correlation between results from the two models for each discharge is poor, indicating differences in the current profile obtained from different EP transport models.

further enhanced for the low toroidal field (i.e. large Larmor radius and orbit width) encountered on NSTX. Consistently with the kick model framework, more comprehensive insight on particle's response to the instabilities can be achieved by interpreting particle's motion caused by instabilities in terms of phase-space variables, as shown in figures 5(*c*)–(*e*) for a $n = 4$ TAE on NSTX. Panels (*c*) and (*d*) in figure 5 show the root-mean-square energy kicks experienced over 10 μs by fast ions based on their (E, P_ζ, μ) variables. Particles that lose (gain) energy are pushed to smaller (larger) P_ζ, as inferred from a representative kick probability $p(\Delta E, \Delta P_\zeta)$ shown in figure 5(*e*), which reflects the overall relation $\Delta P_\zeta/\Delta E \sim n/\omega$ for resonant particles [12]. Since $P_\zeta \propto -\Psi$, kicks results in an outward (inward) motion as P_ζ decreases (increases). In the simplified treatment adopted for the kick model, mode properties such as frequency and radial structure are assumed to be

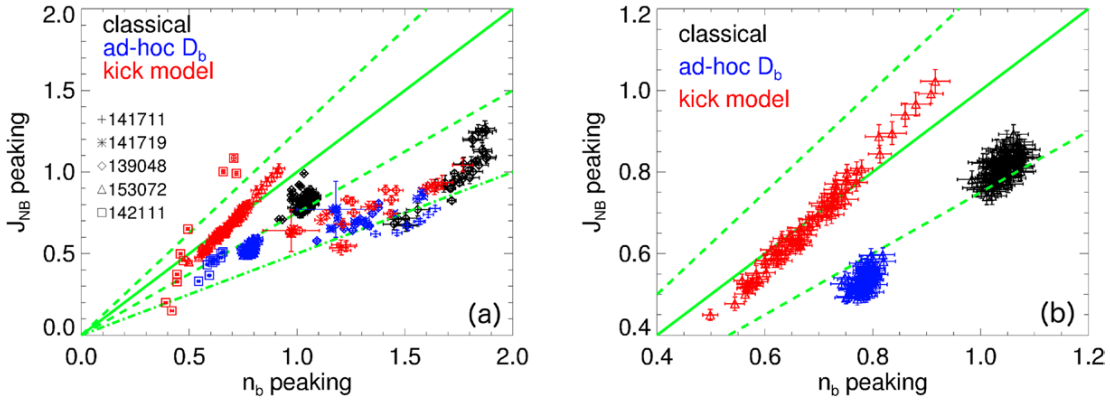

Figure 8. (*a*) Peaking of NB driven current with respect to peaking of NB ion density. Colors refer to classical simulations (black) and to runs using ad hoc diffusivity (blue) or the kick model (red) to account for enhanced NB ion transport. (*b*) Detail from panel (*a*) for DIII-D discharge #153072, showing the correlation between $J_{\rm NB}$ and n_b profiles that can result from the kick model.

constant. Therefore, a de-tuning of the particle's motion from the resonance will eventually occur for large E and P_ζ variations from their original values.

More details on modeling results for the distribution function can be found elsewhere [36]. These observations can be expected to imply differences for other quantities that result from integrals of the fast ion distribution over phase space variables.

4.2. Radial profiles

Experimentally, Alfvénic instabilities are known to cause flattening and reduction in the beam ion density, n_b (see, for example, [37]). Information on the radial profile of the NB driven current is much more difficult to obtain directly from the experiments, and analysis through codes such as TRANSP is required. Figure 6 shows a comparison of the peaking factor computed for the NB driven current, $J_{\rm NB}$, based on the three assumptions for fast ion transport. The peaking factor is computed as the ratio between central current to its average over the entire minor radius.

As a general result from the NSTX/DIII-D database, peaking is reduced by up to a factor 2 with respect to *classical* simulations, indicating a net redistribution of current towards larger minor radii. On average, the two transport models predict a comparable broadening of the $J_{\rm NB}$ profile. However, as expected from the differences observed in the fast ion distribution function, the radial profiles of the NB-driven current obtained with the two models can be quite different (figures 6(*b*) and (*c*)). This results from the phase space selectivity of the kick model, not present in the ad hoc model. Figure 7 shows a direct comparison of the peaking factor computed through the two transport models. For most discharges, the ad hoc model predicts small variations of the peaking at different times, as expected from the radial uniformity of D_b. The kick model results exhibit variations over a broader range, since different modes (with different radial structure) can be active at different times.

Implications are not limited to the non-inductive current profile. Since the total current is imposed in these analyses,

Table 2. Correlation coefficients between $J_{\rm NB}$ and n_b peaking factors for each discharge in the database using results from classical simulations and simulations using ad hoc D_b and kick model for EP transport.

Device	Shot no.	$R_{\rm class}$	$R_{\rm adhoc}$	$R_{\rm kick}$	$N_{\rm samp}$
NSTX	139048	0.86 ± 0.05	0.94 ± 0.04	0.90 ± 0.06	10
NSTX	141711	0.73 ± 0.60	0.98 ± 0.05	0.96 ± 0.10	8
NSTX	141719	0.86 ± 0.27	0.91 ± 0.01	0.99 ± 0.08	14
DIII-D	142111	0.98 ± 0.01	0.89 ± 0.02	0.95 ± 0.01	10
DIII-D	153072	0.50 ± 0.25	0.79 ± 0.31	0.97 ± 0.05	84

Note: The last column reports the number of samples used to compute the correlation for each discharge.

variations of $J_{\rm NB}(r)$ automatically imply changes in the ohmic current profile as well. The bootstrap current is not affected, since thermal plasma profiles are given as input in the simulations. Different ohmic current profiles, in turn, result in changes in the ohmic heating, which can be a significant source term for the overall (local) power balance. (Incidentally, it is noted that even larger variations in the predicted quantities can be expected for *predictive* simulations, for which total current, q-profile and magnetic configuration may not be imposed as input but computed self-consistently).

Further differences in the TRANSP results are observed from a combined analysis of the evolution of fast ion density and NB driven current profiles, see figure 8. A broadening is predicted in both quantities, with significant reduction of the fast ion density peaking with respect to classical simulations. An important feature is the different correlation between $J_{\rm NB}$ and fast ion density evolution that can result from the two transport models. Figure 8(*b*) shows an example from the high-$q_{\rm min}$, nearly steady-state DIII-D discharge #153072, for which $J_{\rm NB}$ and n_b peaking computed with the kick model align along a (roughly) straight line over an extended range of peaking values. For this specific discharge, the correlation computed for simulations based on either classical or ad hoc diffusive transport hypotheses is weaker. A plausible interpretation of this result invokes the relation $\Delta P_\zeta/\Delta E \sim n/\omega$ that subsists between energy and P_ζ changes induced by an instability with toroidal mode number n and angular frequency ω

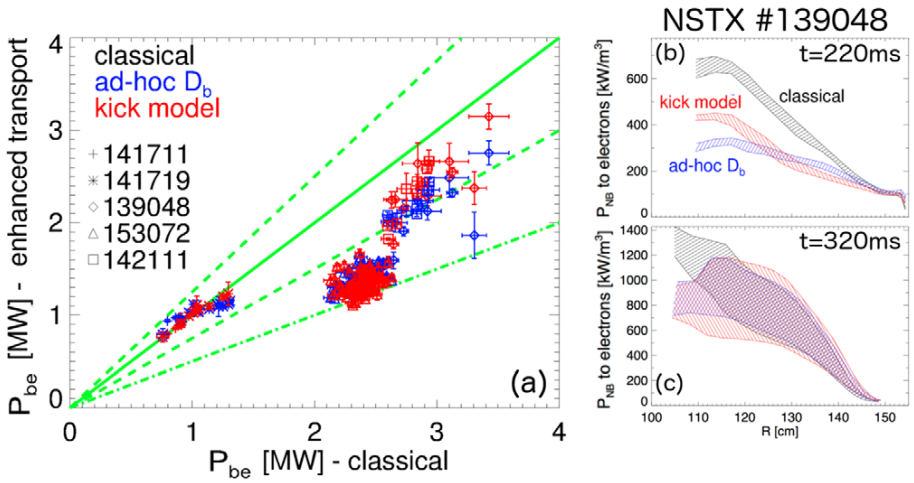

Figure 9. (*a*) Comparison of NB power flowing to thermal electrons, P_{be}, from classical simulations and from runs using ad hoc diffusivity (blue) or the kick model (red). ((*b*) and (*c*)) Radial profiles of NB power to electrons for NSTX discharge #139048 around 220 and 320 ms. Similar to the profiles of J_{NB} shown in figures 6(*b*) and (*c*), differences in the P_{be} profiles between ad hoc D_b and kick models are, in general, a strong function of time.

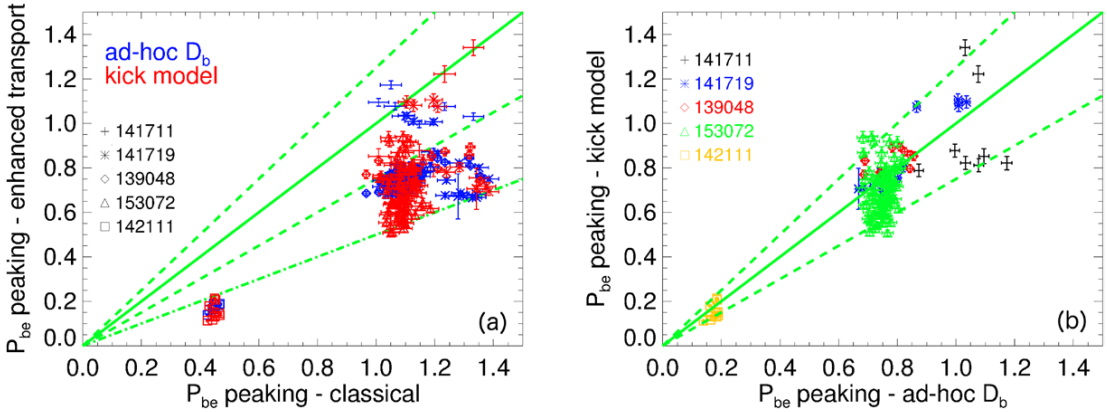

Figure 10. (*a*) Comparison of P_{be} profile peaking from ad hoc D_b and kick models with respect to classical simulations. (*b*) Although the average peaking factor is similar for the two models, temporal variations can be quite different, as inferred from the poor correlation between peaking factors for each discharge.

[12]. Neglecting corrections for the screening electron current [35], take

$$J_{NB}(\Psi) \sim \int v_{\parallel} f(E,p,\Psi)\,\mathrm{d}E\,\mathrm{d}p \qquad (1)$$

$$n_b(\Psi) \sim \int f(E,p,\Psi)\,\mathrm{d}E\,\mathrm{d}p \qquad (2)$$

and consider the definition of $P_\zeta \equiv -\Psi + f(v_\parallel)$, where $v_\parallel = p\sqrt{E}$ (p: pitch). For similar mode numbers n and low frequency $\omega \to 0$, instabilities will cause finite ΔP_ζ with negligible ΔE. In terms of radial profiles, this implies a finite radial transport *of resonant particles* with negligible change of energy. If the resonant particles are the same that mostly sustain the NB driven current, the $\omega \to 0$ limit thus leads to $J_{NB}(\Psi) \propto n_b(\Psi)$ from equations (2) since $v_\parallel \approx$ const.. (The opposite limit $\omega \to \infty$ would cause finite $J_{NB}(\Psi)$ changes with negligible changes in the n_b profile). DIII-D discharge #153072 features large-amplitude, low-frequency AEs (figure 1), which contribute to $\gtrsim$50% of the observed drop in neutron rate. Based on the above discussion, it is argued that those low-frequency modes are mostly responsible for the correlation between J_{NB} and n_b.

Table 2 reports the correlation coefficients between J_{NB} and n_b peaking factors computed for all discharges in the database and for each run (based on classical, ad hoc D_b and kick model for EP transport). For most of the other discharges, the correlation between J_{NB} and n_b peaking is more elusive. Similar coefficients are computed for the ad hoc D_b and kick models, once uncertainties in the correlation coefficient are taken into account. Moreover, classical simulations also show a significant correlation, although uncertainties are larger. The reasons for the much less conclusive results from other discharges than DIII-D #153072 are believed to be of both physics and numerical nature. On the physics side, low-frequency modes typically play a smaller role in EP transport (except for bursts of kink-like modes on NSTX), so changes in E and P_ζ can be equally important. In addition, plasma scenarios are not as

stationary as DIIID #153072, and the effects of instabilities are smaller (as deduced from the smaller neutron rate drop in figure 1). A stronger role of fast ion distribution source/sink terms versus time than in DIII-D #153072 can then be expected, which complicates the interpretation of equations (2) as time evolves in terms of J_{NB}, n_b peaking versus instabilities. On the numerical side, the number of samples from which correlation coefficients are computed for each discharge is in general much smaller than for DIIID #153072, so it is more difficult to separate the effects of instabilities from those of other time-varying background quantities. More analysis is therefore required to assess the generality of these results. However, they suggest that the correlation between energy and canonical angular momentum changes induced by resonant instabilities [12], which is included in the kick model, can also propagate to integrated quantities.

4.3. Power balance

As a final example of the effects of fast ion modeling on results from integrated simulations, figure 9(*a*) shows the computed power transferred through thermalization from the slowing-down NB ions to the thermal electron population, P_{be}, for the same database presented above. When additional fast ion transport is included in the simulations, a reduction of up to ~2 in the power with respect to *classical* simulations is computed. A similar reduction is observed in the power flowing from NB ions to thermal ions, not shown in the figure. Similar to the results for NB driven current profiles, the overall reduction is comparable for the two transport models compared here, but the radial profiles can be substantially different as shown in figures 9(*b*) and (*c*) for NSTX discharge #139048. Further evidence for differences in the profiles predicted by the two models is shown in figure 10. Average peaking factors are comparable for the two models (figure 10(*a*)). However, a direct comparison reveals that no systematic relationship exists between the two datasets (figure 10(*b*)), i.e. profiles follow a different time evolution for the two models.

The lack of global trends for P_{be} among all discharges in the database, see figures 9 and 10, may suggest that the deficiency in P_{be} is strongly dependent on the details of the instabilities or D_b used for each discharge. As for the results on $J_{NB}(r)$ presented in figure 3, this is the case for the radial profiles, but once integrated over radius a trend appears between the total P_{be} and the neutron rate deficit. Figure 11 shows the rather smooth trend among all discharges of total P_{be} relative to classical simulations versus neutron rate deficit. The only outlier is DIII-D discharge #142111, which features a large neutron rate deficit $\geqslant$50% but relatively small decrease in the total P_{be} with respect to classical. The reason for this departure from the general trend is, at present, not clear.

As mentioned in section 4.2, other heat source terms besides NB thermalization power, such as the ohmic current profile, are also modified depending on the NB ion transport model adopted. This potentially large difference in source terms can lead to profound differences in a power balance analysis, e.g. to estimate the local thermal diffusivities. In

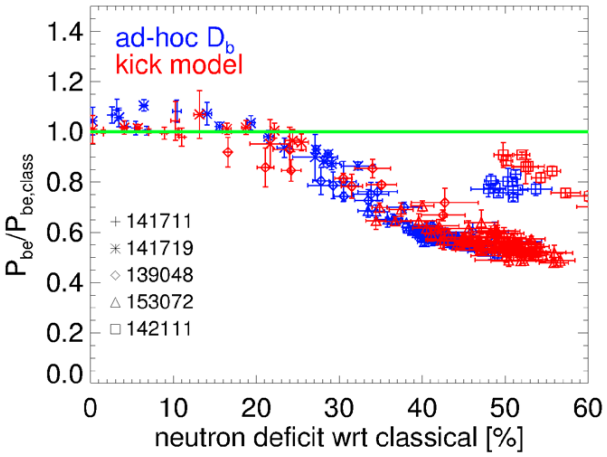

Figure 11. Total NB power thermalizing on electrons, P_{be}, normalized to its classical value as a function of neutron rate deficit. Data refer to the ad hoc model (blue) and to the kick model (red).

general, the use of different fast ion transport models has more ramifications than it could appear at a first glance. One advantage of implementing improved fast ion transport models in codes such as TRANSP is that those secondary effects and multiple feedback loops can be taken into account consistently. One notable exception, however, is that no terms are included yet in NUBEAM/TRANSP to account for the power stored in the modes themselves or for the power damped by the modes on the thermal plasmas, e.g. through ion/electron Landau damping. In addition to the power lost by escaping ions (which is included in the modeling), the two terms can account for a significant fraction of the power associated with fast ions and instabilities. For typical mode amplitudes observed on the two devices, for example, the power stored in each mode can easily account for tens of *kW*. Work is in progress to assess the possibility to include these additional terms in the global TRANSP power balance, although this would require a rigorous model accounting for the localization of some mode damping mechanisms. This is required since plasma parameters in a time-dependent TRANSP simulation can vary substantially as a function of time. Damping terms (e.g. electron and ion Landau damping) through which modes transfer energy to the thermal plasma should be computed based on the thermal plasma parameters as a function of time. Moreover, localized modes can sample limited regions of the plasma, thus leading to different values of damping, i.e. of power flow. Therefore, the radial structure of the modes (even if assumed to be fixed and equal to its ideal MHD structure) should also be taken into account in a consistent, time dependent computation of the power balance. This seems, at present, beyond the TRANSP capabilities.

5. Conclusions

Integrated simulations of tokamak discharges based on classical fast ion physics have been compared to simulations including enhanced fast ion transport by plasma instabilities through two different models implemented in the TRANSP

code. The key difference between the two models is whether fast ion transport is limited to a simple radial diffusion or it includes phase space modifications. A database from NSTX and DIII-D discharges featuring robust MHD activity has been selected to assess the generality of the results.

The two transport models generally lead to similar predictions for global quantities such as neutron rate, stored energy and NB current drive efficiency. (In fact, the first two quantities—and especially the measured neutron rate—are often used to calibrate the free parameters of the models). This justifies the use of the simpler ad hoc diffusive model for routine analysis, e.g. to compare discharges in terms of overall performance (see, for example, [38, 34, 39, 30, 40]). It also confirms the validity of recent upgrades to the simple diffusive model in TRANSP, which now accepts a target neutron rate waveform as input and adjusts the diffusion coefficient during the run to match the input [41]. The latter feature is certainly useful for rapid analysis, e.g. to guide decisions during an experimental session when time for in-between-shots analysis is limited.

The main differences between the two models arise in the radial profiles of quantities resulting from integrals of the fast ion distribution function. A first reason for this is that a spatially uniform diffusivity has been used herein for the ad hoc model. In principle, a radial dependence $D_b(r)$ can be provided as input to TRANSP. However, there are no rigorous criteria to select a specific radial profile for an ad hoc parameter such as D_b. On the contrary, the radial dependence (through the P_ζ phase space variable) is implicit in the kick model probabilities, which are computed based on the radial mode structure of the observed instabilities.

A second reason for different results from the two models is the possible correlation between energy and P_ζ variations, resulting from the resonant nature of the wave-particle interaction [12], which is included in the kick model. That same relationship can also lead to important correlations between different quantities and their temporal evolution, for example between NB driven current profile and beam ion density, that are not reproducible by the simple diffusive model. The presence—and strength—of such correlations appear to depend on the character and strength of the instabilities observed in each discharge, which are included in the transport probabilities in NUBEAM through the kick model. For example, from the database analyzed in this work correlations are clear for a DIII-D discharge featuring strong activity of low-frequency Alfvénic modes which account for $\gtrsim$50% of the overall 40–60% drop in neutron rate with respect to *classical* simulations. However, correlations are more elusive for other cases that exhibit either less stationary profiles, smaller neutron rate drops and/or higher frequency instabilities. A broader database is therefore required to confirm or reject the generality of those correlations.

As a first step, this work has focused on the analysis of discharges from existing devices. It can be expected that discrepancies in the results based on the different fast ion transport models can be further amplified when the TRANSP code is used in *predictive* mode. In that case, the reduced number of constraints translates in an increased number of unknowns in the simulation, which must be computed self-consistently. Exploration of the potential of the kick model for more consistent predictive runs when MHD instabilities are expected to be destabilized will be the subject of future work. The potential of the kick model to provide more reliable predictions also calls for a more stringent validation of the model against experimental data. Work is in progress to compare predicted EP distribution function properties with available data from the experiments, e.g. from Fast Ion D-Alpha diagnostics, Neutral Particle analyzers and fast ion loss detectors.

Acknowledgments

Contributions from—and useful discussions with—members of the NSTX-U and DIII-D Energetic Particle groups are kindly acknowledged. We thank Dr. S.A. Sabbagh (Columbia University) for EFIT analysis of NSTX discharges, and for clarifying discussions on the interpretation of EFIT results. This work was supported by the US DOE Office of Science under Contract Number DE-AC02-09CH11466. NSTX-U at Princeton Plasma Physics Laboratory (Princeton University, New Jersey—USA) is a DOE Office of Science User Facility. The digital data for this paper can be found in http://arks.princeton.edu/ark:/88435/dsp018p58pg29j.

References

[1] Fasoli A. *et al* 2007 Progress in the ITER physics basis. chapter 5: physics of energetic ions *Nucl. Fusion* **47** S264
[2] Hawryluk R. 1979 An empirical approach to tokamak transport *Physics of Plasmas Close to Thermonuclear Conditions, Proc. from the Int. School of Plasma Physics (Villa Monastero, Varenna, Italy 27 August–8 September)*
[3] More details on the TRANSP code available at http://w3.pppl.gov/pshare/help/transp.htm
[4] Ono M. *et al* 2000 *Nucl. Fusion* **40** 557
[5] Luxon J.L. 2005 *Fusion Sci. Technol.* **48** 828
[6] Lao L.L. *et al* 1985 *Nucl. Fusion* **25** 1611
[7] Sabbagh S.A. *et al* 2001 *Nucl. Fusion* **41** 1601
[8] Pankin A. *et al* 2004 *Comput. Phys. Commun.* **159** 157
[9] Goldston R.J. *et al* 1981 *J. Comput. Phys.* **43** 61
[10] Podestà M. *et al* 2014 *Plasma Phys. Control Fusion* **56** 055003
[11] Podestà M. *et al* 2015 *Nucl. Fusion* **55** 053018
[12] White R.B. 2014 *The Theory of Toroidally Confined Plasmas* 3rd edn (London: Imperial College Press)
[13] White R.B. *et al* 1984 *Phys. Fluids* **27** 2455
[14] Cheng C.Z. 1992 *Phys. Rep. 211* **1** 1
[15] Fu G.Y. *et al* 1993 Stability of the toroidicity-induced Alfvén eigenmode in axysimmetric toroidal equilibria *Phys. Fluids* B **5** 4040
[16] Gorelenkov N.N. *et al* 1999 *Phys. Plasmas* **6** 2802
[17] Van Zeeland M.A. *et al* 2006 *Phys. Rev. Lett.* **97** 135001
[18] Fredrickson E.D. *et al* 2009 *Phys. Plasmas* **16** 122505
[19] Podestà M. *et al* 2012 *Nucl. Fusion* **52** 094001
[20] Podestà M. *et al* 2015 Effects of fast ion phase space modifications by instabilities on fast ion modeling *14th IAEA Technical Meeting on Energetic Particles in Magnetic Confinement Systems O-01 (Vienna, Austria 1–4 September)* www-naweb.iaea.org/napc/physics/meetings/TM49508/website/
[21] Gorelenkov N.N. *et al* 2015 Validating predictive models for fast ion profile relaxation in burning plasmas *14th IAEA Technical Meeting on Energetic Particles in Magnetic Confinement Systems, O-06 (Vienna, Austria 1–4 September)* www-naweb.iaea.org/napc/physics/meetings/TM49508/website/

[22] Carolipio E.M. *et al* 2002 *Nucl. Fusion* **42** 853
[23] Fredrickson E.D. *et al* 2013 *Nucl. Fusion* **53** 013006
[24] Darrow D.S. *et al* 2013 *Nucl. Fusion* **53** 013009
[25] Liu D. *et al* 2015 *Phys. Plasmas* **22** 042509
[26] Van Zeeland M.A. *et al* 2011 *Phys. Plasmas* **18** 056114
[27] Spong D.A. *et al* 2012 *Phys. Plasmas* **19** 082511
[28] Spong D.A. 2013 *Nucl. Fusion* **53** 053008
[29] Todo Y. *et al* 2015 *Nucl. Fusion* **55** 073020
[30] Heidbrink W.W. *et al* 2014 *Plasma Phys. Control. Fusion* **56** 095030
[31] Holcomb C.T. *et al* 2015 *Phys. Plasmas* **22** 055904
[32] Sabbagh S.A. *et al* 2004 *Nucl. Fusion* **44** 560
[33] Sabbagh S.A. *et al* 2006 *Nucl. Fusion* **46** 635
[34] Gerhardt S.P. *et al* 2011 *Nucl. Fusion* **51** 033004
[35] Lin-Liu Y.R. *et al* 1997 *Phys. Plasmas* **4** 4179
[36] Podestà M. *et al* 2016 *Phys. Plasmas* **23** 056106
[37] Heidbrink W.W. *et al* 2007 *Phys. Rev. Lett.* **99** 245002
[38] Baranov Y.F. *et al* 2009 *Plasma Phys. Control. Fusion* **51** 044004
[39] Turnyanskiy M. *et al* 2013 *Nucl. Fusion* **53** 053016
[40] Klimek I. *et al* 2015 *Nucl. Fusion* **55** 023003
[41] Kaye S.M. 2015 Princeton Plasma Physics Laboratory private communication